Int. J. Electron. Commun. (AEÜ) 145 (2022) 154101

Contents lists available at ScienceDirect

International Journal of Electronics and Communications

journal homepage: www.elsevier.com/locate/aeue

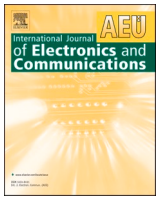

Short communication

Bit error probability of VLC systems in underground mining channels with imperfect CSI

Pablo Palacios Játiva [a], Cesar A. Azurdia-Meza [a,*], David Zabala-Blanco [b], Carlos A. Gutiérrez [c], Iván Sánchez [d], Francisco R. Castillo-Soria [c], Fabian Seguel [e]

[a] Department of Electrical Engineering, Universidad de Chile, Santiago 8370451, Chile
[b] Department of Computing Science and Industry, Universidad Católica del Maule, Talca 3480112, Chile
[c] Faculty of Science, Universidad Autónoma de San Luis Potosí, S.L.P., Mexico
[d] Department of Telecommunications Engineering, Universidad de Las Américas, Quito 170503, Ecuador
[e] Department of Electrical Engineering, Universidad de Santiago de Chile, Santiago 9170124, Chile

ARTICLE INFO

Keywords:
Bit error probability
Channel state information
Least squares channel estimator
Underground mining
Visible light communication

ABSTRACT

Analytical expressions of the statistical distribution of the underground mining visible light communication (UM-VLC) square-channel gain are derived considering scattering, shadowing, and a random position and orientation of the receiver. These expressions are employed to compute the system's bit error probability (BEP) considering shot and thermal noises, on–off keying modulation, as well as perfect and imperfect channel state information (CSI) at the receiver side. The results obtained for the BEP are validated by computer simulations for various UM-VLC scenarios. A close agreement is observed between the analytical and simulated curves. Furthermore, the performance of the UM-VLC system improves by increasing the field-of-view (FoV) and/or signal-to-noise-ratio. Indeed, for a FoV value of 45° for both the UM-VLC system with perfect CSI and imperfect CSI, the best performance in terms of BEP is obtained. In terms of the UM-VLC system with imperfect CSI, BEP curves saturate for higher values of signal-to-noise-ratio (SNR) due to lower values of FoV, specifically in the case of 45°. Finally, the performance of the UM-VLC system increases significantly for higher values of SNR, specifically in the case of 20 dB.

1. Introduction

Compared to traditional indoor environments, the design and implementation of underground mining (UM) visible light communication (VLC) systems is more challenging. This is due to the positioning, tilt, and rotation of the light-emitting diodes (LEDs) and photodiodes (PDs) that interfere with the line of sight (LoS) link, the irregular walls that affect the optical reflections in the non-line of sight (non-LoS) links, the mobile objects that generate shadowing, and dust particles that produce scattering of the optical signal [1]. Furthermore, shot and thermal noises cause degradation of the received signal [1]. The aforementioned factors generate a high bit error probability (BEP); therefore, an in-depth analysis of the performance of UM-VLC systems is required [2,3].

The UM-VLC channel gain fluctuates in the time domain due to the physical variables that compose it. To mitigate this impairment, a widely applied strategy is to estimate the channel state information (CSI) at the optical receiver, by considering the random and probabilistic nature of the channel. Several works with these considerations have been reported in the literature. In [4], the authors propose an interference mitigation scheme by employing a constrained field-of-view angular diversity receiver (CFoV-ADR) and channel estimation based on the least square (LS) approach. Despite considering an indoor multiple-input-multiple-output (MIMO) VLC system, the authors assume the VLC channel to be deterministic in nature. Whereas in [5–7], a performance analysis of indoor VLC systems in terms of error probability and bit error rate (BER), both for single-input–single-output (SISO) and MIMO systems, is presented. Imperfect CSI is considered by generalizing the error or by utilizing the LS method. In addition, variables such as user mobility and PD orientation are considered in the channel model. However, the channel only considers the LoS component, namely an ideal VLC channel.

In terms of the most relevant and recent works reported in the literature describing UM-VLC channel models, in [8,9], a path loss model for a VLC channel applied to mines is proposed. In both works, the

* Corresponding author.
E-mail address: cazurdia@ing.uchile.cl (C.A. Azurdia-Meza).

https://doi.org/10.1016/j.aeue.2021.154101
Received 12 October 2021; Accepted 27 December 2021
Available online 5 January 2022

channel model is based on the well-known Lambertian optical model for indoor environments, where the LoS and NLoS components are considered. Both manuscripts demonstrate that the path loss exhibits a linear behavior in the log-domain. However, their results are based on a channel model that does not include in its analytical expression the main components that affect underground mining tunnels. In [10], the analysis of a VLC system applied to tunnels is characterized. The adopted model is the Lambertian VLC channel model with the LoS and diffuse components. The VLC system performance is evaluated in terms of Symbol Error Rate (SER). Despite the fact that its results are obtained by simulating a tunnel scenario, the channel model limits them because it does not consider factors such as shadowing or scattering, and the receiver assumes perfect CSI. In [11], a VLC channel model that considers dust particles is presented. The scenario is analyzed using a Lambertian VLC channel model by considering LoS and non-LoS components, and the results are presented in terms of the CIR. However, the limitation of this work is not to include the effect of scattering directly in the theoretical model of the channel.

In [12], the analysis on a VLC system applied to underground mines is presented. The effect of shadowing and scattering are analyzed as channel-independent phenomena. Consequently, the effects of these phenomena are not included in the analytical model of the VLC channel, so this omission would be its main limitation. The channel model is based again on the Lambertian optical scheme with LoS and non-LoS components. Therefore, angular variations of transmitter and receiver, and the effect of non-flat walls are not considered neither. The channel is evaluated in terms of the path loss and RMS delay spread. Finally, in [13], a neural network based approach is applied to derive an UM-VLC channel model. The authors assumed a dynamic non-linear behavior of the optical channel. The work is experimentally validated in a dark gallery with a curved roof that emulates a mining tunnel. The main contribution of this article is the estimation of the parameters used for the neural network. However, a disadvantage of this propose is that the model does not consider the scattering or shadowing phenomena in the estimated coefficients.

Based on previous literary analysis on channel estimation methods and UM-VLC channel models, to the best of our knowledge, the BEP of UM-VLC systems subject to a precise statistical channel model with imperfect CSI has not been analyzed in the literature. Therefore, this paper presents a comprehensive performance analysis of a UM-VLC system corrupted by shot and thermal noises. Based on the IEEE 802.15.7 standard and employing PHY-I mode, on–off keying (OOK) modulation is adopted for the transmission of symbols and the LS estimator is implemented in the receiver side [14].

Our contributions can be summarized as follows: (a) The probability distribution function (PDF) expression of the UM-VLC square-channel gain in terms of LoS, non-LoS, and scattering channel components through independent probabilistic factors, that correspond to the random position and orientation of the receiver, and shadowing is obtained. (b) An analytical error-rate analysis for the UM-VLC system, simultaneously affected by the aforementioned factors and imperfect CSI, is presented to derive the BEP expressions for OOK modulation based on the IEEE 802.15.7 standard. (c) A performance analysis of the UM-VLC system with perfect and imperfect CSI in terms of the FoV is presented.

The structure of the article is depicted as follows. The VLC system model applied to UM along with the UM-VLC channel components, the derivation of the PDF from their quadratic forms, and the least squared method are explained in Section 2. The BEP analytical derivation and its respective closed-form expressions are presented in Section 3. In Section 4, the numerical results obtained through computer simulations are shown and discussed. Finally, conclusions are given in Section 5.

2. System Model

We consider a SISO UM-VLC downlink system, as shown in Fig. 1. This scenario includes shadowing produced by moving objects, scattering by dust particles, and light reflections from irregular walls. A single LED positioned and oriented between the ceiling and the wall serves a randomly positioned user within the LED coverage area. We assume that the UM-VLC system is affected by the user's random position, the random orientation of a PD-based receiver located in the user's helmet, shadowing effects characterized by a Poisson process, and imperfect CSI. Data transmission is based on the IEEE 802.1.5.7 standard, employing the PHY-I mode and OOK modulation [14], whereas the receiver employs symbol-by-symbol detection. Consequently, the received signal, r, is expressed as [1,2]

$$r = h_m s + n_m, \tag{1}$$

where s denotes the transmitted symbol, h_m represents the UM-VLC channel-gain coefficient, and n_m stands for the noise affecting the UM-VLC system. Furthermore, $n_m = n_s + n_t$, $n_s \sim \mathcal{N}(0,\sigma_s^2)$, and $n_t \sim \mathcal{N}(0,\sigma_t^2)$, being σ_s^2 and σ_t^2 the variances of the shot noise, n_s, and thermal noise, n_t, respectively [1,15].

2.1. Mathematical model of the UM-VLC channel gain

Based on the UM-VLC channel model proposed in [1], the

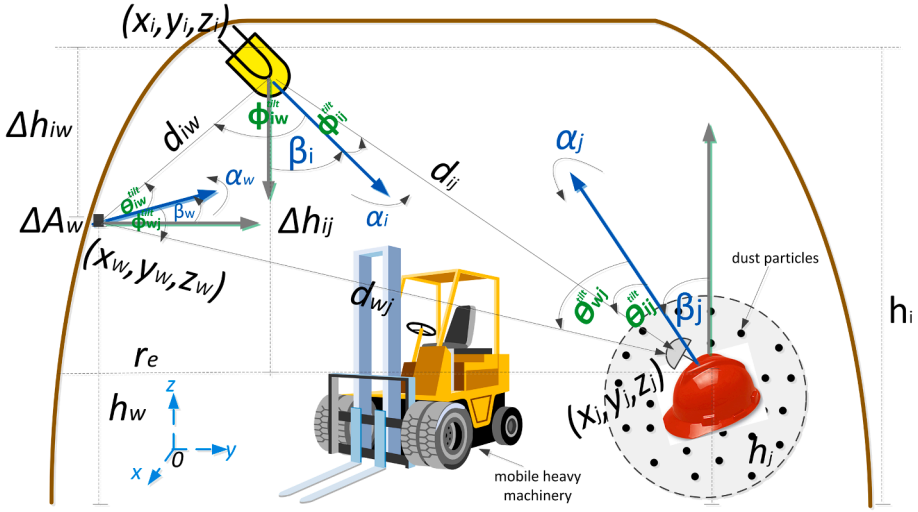

Fig. 1. Downlink light propagation geometry for the UM-VLC system.

instantaneous UM-VLC channel gain, h_m, can be written as [1]

$$h_m = h_{LoS} + h_{NLoS}^{(1)} + h_{sca}, \tag{2}$$

where $h_{LoS}, h_{NLoS}^{(1)}$, and h_{sca} are the channel gains of the LoS link, the non-LoS link due to wall reflections, and a non-LOS link due to dust scattering, respectively. The channel gains h_{LoS} and $h_{NLoS}^{(1)}$ are subject to shadowing [1]. For simplicity, in expression (2) we do not denote time dependency. However, it must be considered that the expression and its variables are time dependent. After restructuring the channel gain components in terms of the variables of interest (random position and orientation of the receiver, and shadowing) and the geometry of the UM scenario, the instantaneous channel gain of the LoS link (h_{LoS}) is given by

$$h_{LoS} = \overbrace{\frac{(m+1)A_p G_r}{2\pi}}^{h_{c_1}} \overbrace{\frac{C_2\left(\frac{C_1}{C_2}+r_m\right)}{\left(r_m^2+\Delta h_{ij}^2\right)^{m+2/2}}}^{h_{r_{m_1}}} \overbrace{\cos\left(\theta_{ij}^{tilt}\right)\mathrm{rect}\left(\frac{\theta_{ij}^{tilt}}{\Theta}\right)^{h_{\theta_{ij}^{tilt}}}}^{P_{ij}^{h_{p_1}}}, \tag{3}$$

where A_p is the active area of the PD, θ_{ij}^{tilt} denotes the incidence angle, $G_r = T_s(\theta_{ij}^{tilt})g(\theta_{ij}^{tilt})$ represents the combined gain of the optical filter and optical concentrator, respectively, and r_m is the distance from the center of the optical cell to the receiver. Furthermore, Δh_{ij} is the difference in height between the LED and PD, $m = -1/\log_2[\cos(\Phi_{i1/2})]$ is the Lambertian mode number of the LED, which is a function of semi-angle at half power ($\Phi_{i1/2}$), P_{ij} is the probability that the LoS optical link is not blocked [1], Θ is the FoV of the PD, and $\mathrm{rect}\left(\theta_{ij}^{tilt}/\Theta\right) = 1$ is a decision function, such that $0 \leqslant \theta_{ij}^{tilt} \leqslant \Theta$ and 0 otherwise. The respective constants' values are given as $C_1 = \Delta h_{ij}\cos^m(\beta_i) - x_i\sin^m(\beta_i)\cos^m(\alpha_i) - y_i\sin^m(\beta_i)\sin^m(\alpha_i)$ and $C_2 = \cos(\theta_m)\sin(\beta_i)\cos(\alpha_i) + \sin(\theta_m)\sin(\beta_i)\sin(\alpha_i)$, where (x_i, y_i) is the x-y LED location in Cartesian coordinates, β_i is the LED tilt angle with respect to the z-axis, α_i is the LED rotation angle with respect to the x-axis, and θ_m is the user's angular position within the LED coverage area.

The instantaneous gain of the first reflection of the non-LoS link $h_{NLoS}^{(1)}$ is given by

$$h_{NLoS}^{(1)} = \overbrace{\frac{(m+1)A_p G_r \Delta A_w \rho_w \cos^m\left(\phi_{iw}^{tilt}\right)\cos\left(\theta_{iw}^{tilt}\right)}{2\pi\left(r_e^2+\Delta h_{iw}^2\right)}}^{h_{c_2}} \underbrace{\frac{C_4\left(\frac{C_3}{C_4}+r_m\right)}{\left((r_e+r_m)^2+\Delta h_{wj}^2\right)^{1/2}}}_{h_{r_{m_2}}} \overbrace{\times\underbrace{\cos\left(\theta_{wj}^{tilt}\right)\mathrm{rect}\left(\frac{\theta_{wj}^{tilt}}{\Theta}\right)}_{h_{\theta_{wj}^{tilt}}}}^{P_{wj}^{h_{p_2}}}, \tag{4}$$

where ΔA_w denotes the area of the reflective element w, whose reflection coefficient and location are represented by ρ_w and (x_w, y_w), respectively. The incidence angle with respect to w and the irradiance angle of the light component reaching w are symbolized with θ_{iw}^{tilt} and ϕ_{iw}^{tilt}, respectively. The angles of incidence and irradiance, denoted by θ_{wj}^{tilt} and ϕ_{wj}^{tilt}, respectively, are measured with respect to the light beam reflected by w toward the PD. Δh_{wj} is the difference in height between w and the PD, Δh_{iw} is the difference in height between the LED and w, r_e is the maximum coverage radius of the LED, which we assume to coincide with the wall position where w is located. P_{wj} represents the probability that the non-LoS optical link is not blocked [1]. The constant's values are $C_3 = -\Delta h_{wj}\cos(\beta_w) - x_w\sin(\beta_w)\cos(\alpha_w) - y_w\sin(\beta_w)\sin(\alpha_w)$ and $C_4 = \cos(\theta_m)\sin(\beta_w)\cos(\alpha_w) + \sin(\theta_m)\sin(\beta_w)\sin(\alpha_w)$, where β_w is the w tilt angle with respect to the z-axis and α_w is the rotation angle with respect to the x-axis.

Finally, the instantaneous channel gain due to dust scattering is given by

$$h_{sca} = \sum_{n=1}^{N} \underbrace{\frac{\overbrace{\frac{C_5 A_p (m+1)}{2\pi}}^{h_{c_3}} \overbrace{\cos\left(\theta_{S_n-j}\right)\mathrm{rect}\left(\frac{\theta_{S_n-j}}{\Theta}\right)^{h_{\theta_{S_n-j}}}}}{\left[\sqrt{C_r + r_m^2 - C_6\left(r_m^2+\Delta h_{ij}^2\right)^{1/2}} + r_n\right]^2}}_{h_{r_{m_3}}}. \tag{5}$$

We consider that within the disk-shaped area centered on the PD, there are N scatterers (S_n), r_n is the distance from the n^{th} scatterer to the PD, and θ_{S_n-j} represents the angle between the distance vector from the n^{th} scatterer to the PD normal vector [1]. The respective values of the constants are given as $C_r = r_n^2 + \Delta h_{ij}^2$, $C_5 = G_n\cos^m(\phi_{i-S_n})$, and $C_6 = 2r_n\cos(\beta_{i-S_n})$, where G_n is a scatter gain coefficient, ϕ_{i-S_n} is the irradiance angle measured between the LED normal vector and the distance vector from the LED to S_n, and β_{i-S_n} denotes the difference between the angles θ_{i-S_n} and θ_{ij}^{tilt} [1]. From ()()()(3)–(5), it is observed that the channel gains can be expressed as a product of factors corresponding to the random position $h_{r_{m_{(\cdot)}}}$ and orientation $h_{\theta_{(\cdot)}}$ of the receiver, shadowing $h_{p_{(\cdot)}}$, and the constant expressions $h_{c_{(\cdot)}}$.

2.2. PDF derivation of the UM-VLC square-channel gain

In order to obtain the analytical BEP expressions [16], first it is necessary to generate the UM-VLC square channel gain and then obtain its PDF [5,16]. Therefore, from (3), the channel gain h_{LoS} can be expressed as the product of the deterministic gain h_{c_1}, the user random

position $h_{r_{m_1}}$, the random receiver-orientation $h_{\theta_{ij}^{tilt}}$, and the shadowing h_{p_1}. To obtain the PDF of the LoS square-channel gain, we define $\Delta_{\theta_{ij}^{tilt}}(a,b) = F_{\theta_{ij}^{tilt}}(b) - F_{\theta_{ij}^{tilt}}(a)$ for the $h_{\theta_{ij}^{tilt}}$ factor, which represents the probability that the random variable θ_{ij}^{tilt} is in the interval $(a,b]$, for $a,b \in \mathbb{R}, a \leqslant b$, blocked by an obstacle, and $\mathbb{E}(p_v)$ is the expected value of p_v [1].

By exploiting the independence of $h_{r_{m_1}}, h_{p_1}$, and $h_{\theta_{ij}^{tilt}}$ [17], we find that the PDF of the LoS square-channel gain is given as

$$f_{h^2_{LoS}}\left(x\right) = \frac{C_l}{h^2_{c_1}}\int_{\mathscr{R}_y}\int_{\mathscr{R}_z}\frac{\exp[-\epsilon\mathbb{E}(p_v)z]}{yz}\left[\frac{f_{\Delta_{r_m}}(B(y,z))}{(m+2)B(y,z)}(yz)^M - \frac{f_{\Delta_{r_m}}\left(\frac{(yz)^{\frac{1}{2}}-C_1}{C_2}\right)}{C_2(yz)^{\frac{1}{2}}}\right]\times\left[f_{\theta_{ij}^{tilt}}(C(x,y,z))\left(\frac{4x}{h^2_{c_1}yz} - \frac{4x^2}{\left(h^2_{c_1}yz\right)^2}\right)^{-\frac{1}{2}} + P_1\left(x,y,z\right)\right]dydz, \tag{9}$$

where $F_{\theta_{ij}^{tilt}}(\cdot)$ is the cumulative distribution function (CDF) of θ_{ij}^{tilt} [16]. The CDF of the LoS square-channel gain, $F_{h^2_{\theta_{ij}^{tilt}}}(x)$, is equal to $F_{h^2_{\theta_{ij}^{tilt}}}(x) = \Delta_{\theta_{ij}^{tilt}}\left(0.5\cos^{-1}(2x-1),\Theta\right) + T_1(\Theta)\mathrm{rect}(x)$, for $0 < x \leqslant 1, F_{h^2_{\theta_{ij}^{tilt}}}(x) = 0$ for $x < 0$, and $F_{h^2_{\theta_{ij}^{tilt}}}(x) = 1$ for $x > 1$, whereas $T_1(\Theta) = 1 - F_{\theta_{ij}^{tilt}}(\Theta)$ [16]. The corresponding PDF is given as

$$f_{h^2_{\theta_{ij}^{tilt}}}\left(x\right) = \frac{C_{\theta_{ij}^{tilt}}}{\sqrt{4x(1-x)}}f_{\theta_{ij}^{tilt}}\left(\frac{\cos^{-1}(2x-1)}{2}\right) + T_1\left(\Theta\right)\delta\left(x\right), \tag{6}$$

defined for $\cos^2(\Theta) \leqslant x < 1$ and 0 otherwise. Furthermore, $C_{\theta_{ij}^{tilt}}$ is a normalization constant and $f_{\theta_{ij}^{tilt}}$ is the PDF of θ_{ij}^{tilt}, which is defined in general form to directly incorporate any probability distribution of θ_{ij}^{tilt}. for $0 < x \leqslant 1$ and $T_1(\Theta)$ for $x = 0$. $C_l = 0.5C_hC_{r_{m_1}}C_{\theta_{ij}^{tilt}}$ with C_h as the normalization constant, $\mathscr{R}_y$ and $\mathscr{R}_z$ are the set of y and z values for which the function to be integrated takes nonzero value, $B\left(y,z\right) = \left((yz)^{\frac{-1}{m+2}} - \Delta h^2_{ij}\right)^{1/2}, C\left(x,y,z\right) = 0.5\cos^{-1}\left(\frac{2x}{h^2_{c_1}yz} - 1\right)$, and $P_1\left(x,y,z\right) = T_1\left(\Theta\right)\delta\left(\frac{x}{h^2_{c_1}yz}\right)$.

From (4), the channel gain $h^{(1)}_{NLoS}$ can be expressed as the product of $h_{c_2}, h_{r_{m_2}}, h_{p_2}$, and $h_{\theta_{wj}^{tilt}}$. Hence, by proceedings as we did to obtain the PDF of $f_{h^2_{LoS}}$, we find that the PDF of the non-LoS square-channel gain, $f_{h^{(1)2}_{NLoS}}(x)$, is given as

$$f_{h^{(1)2}_{NLoS}}\left(x\right) = \frac{C_n}{h^2_{c_2}}\int_{\mathscr{R}_y}\int_{\mathscr{R}_z}\frac{\exp[-\epsilon\mathbb{E}(p_v)z]}{yz}\left[D\left(y,z\right)f_{\Delta_{r_m}}(D(y,z)-r_e) - \frac{f_{\Delta_{r_m}}\left(\frac{E(y,z)-C_3}{C_4}\right)}{C_4E(y,z)}\right]\times\left[\left(\frac{4x}{h^2_{c_2}yz} - \frac{4x^2}{\left(h^2_{c_2}yz\right)^2}\right)^{-\frac{1}{2}} f_{\theta_{wj}^{tilt}}\left(\frac{\cos^{-1}\left(\frac{2x}{h^2_{c_2}yz}-1\right)}{2}\right) + P_2\left(x,y,z\right)\right]dydz, \tag{10}$$

For $h_{r_{m_1}}$, we define $\Delta_{r_m}(a,b)$ as the probability that the random variable r_m is in the interval $(a,b]$. Thereby, $F_{h^2_{r_{m_1}}}(y)$ and $f_{h^2_{r_{m_1}}}(y)$ acquire the form of

$$F_{h^2_{r_{m_1}}}\left(y\right) = \Delta_{r_m}\left(\frac{y^{1/2}}{C_2} - \frac{C_1}{C_2}, A_1\left(y\right)\right), \tag{7}$$

$$f_{h^2_{r_{m_1}}}\left(y\right) = \frac{C_{r_{m_1}}}{2}\left[\frac{y^M f_{\Delta_{r_m}}(A_1(y))}{(m+2)A_1(y)} - \frac{f_{\Delta_{r_m}}(A_2(y))}{C_2y^{1/2}}\right], \tag{8}$$

where $F_{h^2_{r_{m_1}}}(y)$ is defined for $C_1^2 \leqslant y \leqslant (\Delta h_{ij})^{-2(m+2)}$, equal to 0 for $y < C_1^2$, and 1 for $y > (\Delta h_{ij})^{-2(m+2)}$, whereas $f_{h^2_{r_{m_1}}}(y)$ is defined for $C_1^2 \leqslant y \leqslant (\Delta h_{ij})^{-2(m+2)}$ and 0 otherwise. $A_1\left(y\right) = \left(y^{\frac{-1}{m+2}} - \Delta h^2_{ij}\right)^{1/2}$, $A_2\left(y\right) = \frac{y^{1/2}}{C_2} - \frac{C_1}{C_2}, M = \frac{-(m+3)}{m+2}$, and $C_{r_{m_1}}$ is the normalization constant and $f_{\Delta_{r_m}}$ is the PDF of r_m, which is defined in general form to directly incorporate any probability distribution of r_m.

For h_{p_1}, we assume that P_{ij} comes from a Poisson process [1], whose CDF and PDF are given as $F_{h^2_{p_1}}\left(z\right) = \frac{\Gamma((z+1),\epsilon)}{z!}$ and $f_{h^2_{p_1}}(z) = \exp[-\epsilon\mathbb{E}(\mathrm{p_v})z]$ for $z \geqslant 0$. $\Gamma(\cdot,\cdot)$ is the upper incomplete Gamma function, ϵ is the intensity parameter of the Poisson process, p_v is the probability that the LoS is for $0 < x \leqslant 1$ and $T_2(\Theta)$ for $x = 0$, with $T_2(\Theta) = 1 - F_{\theta_{wj}^{tilt}}(\Theta)$. $F_{\theta_{wj}^{tilt}}$ and $f_{\theta_{wj}^{tilt}}$ denote the CDF and PDF of θ_{wj}^{tilt}, respectively, whereas $C_n = 0.5C_hC_{r_{m_2}}C_{\theta_{wj}^{tilt}}, D\left(y,z\right) = \left(\frac{y}{h^2_{c_2}z} - \Delta h^2_{wj}\right)^{-\frac{1}{2}}, E\left(y,z\right) = \left(\frac{y}{h^2_{c_2}z}\right)^{\frac{1}{2}}$, and $P_2\left(x,y,z\right) = T_2\left(\Theta\right)\delta\left(\frac{x}{h^2_{c_2}yz}\right)$.

From (5), the channel gain h_{sca} can be expressed as the sum of the products of $h_{c_3}, h_{r_{m_3}}$, and $h_{\theta_{S_{n-j}}}$. Since the channel component is the sum of multiple statistically independent dispersion components, it is possible to compute the PDF of the square-channel PDF as $f_{h^2_{sca}}(x) = \sum_{n=1}^{N}P(x_n)f_{h^2_{sca_n}}(x_n)$, where $P(x_n)$ is the probability that the n scatterer interacts with the optical link and reaches the receiver and $f_{h^2_{sca_n}}$ is the individual square-channel PDF for the n scatterer. Therefore, it is possible to define $f_{h^2_{sca_n}}$, and consequently $f_{h^2_{sca}}$ by following the same strategy used to derive $f_{h^2_{LoS}}$ and $f_{h^{(1)2}_{NLoS}}$. Hence, $f_{h^2_{sca}}$ is given as

$$f_{h^2_{sca}}\left(x\right) = \frac{C_s}{h^2_{c_3}} \sum_{n=1}^{N} P\left(x_n\right) \int_{\mathscr{R}_y} \left[\left(\frac{4x}{h^2_{c_3} y} - \frac{4x^2}{\left(h^2_{c_3} y\right)^2} \right)^{-\frac{1}{2}} \times f_{\theta_{S_n-j}} \left(\frac{\cos^{-1}\left(\frac{2x}{h^2_{c_3} y} - 1 \right)}{2} \right) + P_3\left(x, y, z\right) \right] \times \left[\frac{F\left(y\right) K_1 y^{\frac{5}{2}} \left(\frac{K_4 F\left(y\right) + K_5 y + y^{\frac{1}{2}}}{\frac{K_1}{4} y} \right)^{\frac{1}{2}}}{F\left(y\right) y + K_6 y^{\frac{5}{2}} + \left(-K_6 y^{\frac{1}{2}} + \frac{K_4}{2} \right) y^2} \right] f_{\Delta_{rn}}\left(G\left(y \right) \right) dy dz, \tag{11}$$

for $0 < x \leqslant 1$ and $T_3(\Theta)$ for $x = 0$, with $T_3(\Theta) = 1 - F_{\theta_{S_n-j}}(\Theta)$. $F_{\theta_{S_n-j}}$ and $f_{\theta_{S_n-j}}$ are the CDF and PDF of θ_{S_n-j}, respectively, $C_s = C_h C_{r_{m_3}} C_{\theta_{S_n-j}}$, $P_3\left(x, y, z\right) = T_3\left(\Theta\right)\delta\left(\frac{x}{h^2_{c_3} y}\right)$, $F\left(y\right) = \left(-K_2 y^2 + K_3 y^2 + y^{\frac{3}{2}} \right)^{\frac{1}{2}}$, $G\left(y\right) = \left(\frac{y^{\frac{1}{2}} + K_5 y + K_4 \left(\left(K_3 - K_2 \right) y^2 + y^{\frac{3}{2}} \right)^{\frac{1}{2}}}{\frac{K_1}{4} y} \right)^{\frac{1}{2}}$, and the respective values of the constants are: $K_1 = 4r_n^4$, $K_2 = r_n^6$, $K_3 = r_n^6 \cos^2(\beta_{i-S_n})$, $K_4 = 2r_n^3 \cos(\beta_{i-S_n})$, $K_5 = 2r_n^6 \cos(\beta_{i-S_n}) - r_n^4 \Delta h_{ij}^2 - r_n^6$, and $K_6 = 4r_n^9 \cos(\beta_{i-S_n}) - 4r_n^9 \cos^3(\beta_{i-S_n})$.

In order to obtain the PDF of the UM-VLC square-channel gain, $f_{h_m^2}$, we must obtain the expression of the square UM-VLC channel gain, h_m^2. Its derivation is obtained by applying basic mathematical operations in the following form:

$$h_m^2 = \left(h_{LoS} + h^{(1)}_{NLoS} + h_{sca} \right)^2, \tag{12}$$

$$h_m^2 = 2h_{LoS}h^{(1)}_{NLoS} + 2h_{LoS}h_{sca} + 2h^{(1)}_{NLoS}h_{sca} + h^2_{LoS} + h^{2(1)}_{NLoS} + h^2_{sca}. \tag{13}$$

Due to the characteristic of the optical signal and its propagation behavior in the UM environment [1], we can deduce that for a given instantaneous time, the h_{LoS} component multiplied with each other component in Eq. (13) will be annulled by their own temporary dispersion. Therefore $2h_{LoS}h^{(1)}_{NLoS} + 2h_{LoS}h_{sca} = 0$. However, the travel time of the $h^{(1)}_{NLoS}$ and h_{sca} components may be the same for some cases, which depend on the receiver position. Hence, this implies that the multiplication performed on the component $2h^{(1)}_{NLoS}h_{sca}$ is close to zero but not zero. In this context, the expression (13) can be rewritten as

$$h_m^2 = h^2_{LoS} + h^{2(1)}_{NLoS} + h^2_{sca} + 2h^{(1)}_{NLoS}h_{sca}. \tag{14}$$

Finally, to obtain $f_{h_m^2}$, we consider the expressions of $f_{h^2_{LoS}}$, $f_{h^{(1)2}_{NLoS}}$, $f_{h^2_{sca}}$, $f_{h^{(1)}_{NLoS}}$, and $f_{h_{sca}}$ by exploiting the independence among them. Hence, the occurrence of one does not affect the probability of occurrence of the other. Therefore, we apply the property of the sum of several probability density functions [18], and the following expression is obtained

$$f_{h_m^2}\left(x\right) = 2\left[f_{h^2_{LoS}}\left(x\right) \otimes f_{h^{(1)2}_{NLoS}}\left(x\right) \otimes f_{h^2_{sca}}\left(x\right) \otimes f_{h^{(1)}_{NLoS}}\left(x\right) f_{h_{sca}}\left(x\right) \right], \tag{15}$$

where $\otimes$ is the convolution operator.

2.3. Channel estimation by the least squares method

Imperfect CSI is a problem that occurs in the receiver of any wireless communication system, which is due to a channel estimation error. This is one of the main problems in achieving optimal detection of the received signal. For our study, we consider both perfect and imperfect CSI. In the case of the imperfect CSI, it is necessary to estimate the effect of the UM-VLC channel on the received optical signal since we assume that the optical receiver does not know the channel information. Therefore, we performed the channel estimation using the LS method [5]. This method allows us to obtain the estimated UM-VLC channel coefficients together with their estimation error. The mathematical analysis of the LS method is simple and its implementation complexity is low compared to other channel estimation methods in the literature [5].

We estimate the channel coefficients h_m by transmitting a sequence of independent pilot symbols, T_s, prior to the transmission of the data, according to the IEEE 802.15.7 standard [14]. Therefore, the received signal vector, $\mathbf{r}_s$, is expressed as $\mathbf{r}_s = h_m \mathbf{s}_s + \mathbf{n}_s$, where $\mathbf{s}_s \in \mathbb{R}^{T_s \times 1}$ is the pilot symbol vector ($\mathbb{R}$ denotes the field of real numbers) and $\mathbf{n}_s = \mathbf{n}_{s(s)} + \mathbf{n}_{t(s)}$, is the additive noise vector, whose components are $\mathbf{n}_{s(s)} \sim \mathscr{N}(\mathbf{0}_{T_s}, \sigma_s^2 \mathbf{I}_{T_s})$, and $\mathbf{n}_{t(s)} \sim \mathscr{N}(\mathbf{0}_{T_s}, \sigma_t^2 \mathbf{I}_{T_s})$, being $\mathbf{0}_{T_s} \in \mathbb{R}^{T_s \times 1}$ the vector of zeros and $\mathbf{I}_{T_s} \in \mathbb{R}^{T_s \times T_s}$ the identity matrix.

The channel coefficient estimated by the LS method is obtained as $\widehat{h}_{m_{ls}} = h_m + \xi_{ls}$, where $\xi_{ls} = \frac{\mathbf{s}_s^T \mathbf{n}_s}{\|\mathbf{s}_s\|^2}$ is the estimation error, such that $\xi_{ls} \sim \mathscr{N}(0, \Gamma_s)$ with $\Gamma_s = \frac{\|\mathbf{s}_s\|^2}{(\sigma_s^2 + \sigma_t^2)}$, and $(\cdot)^T$ is the transpose operator.

To implement a consistent maximum likelihood (ML) rule at the receiver [5], the optimal decision for the UM-VLC system with perfect CSI is given as $\widehat{s} = \text{argmax}_s(2rh_m - s^2)$. Whereas the decision rule for the system with imperfect CSI is given as $\widehat{s} = \text{argmax}_s(2r\widehat{h}_{m_{ls}} - s^2)$.

Table 1
Underground mining VLC scenario features and general simulation parameters.

Parameter	Value
Scenario features	
Scenario size ($w \times l \times h$)	($3 \times 6 \times 5$) m
LED position (x_i, y_i, z_i)	(0.5,3,4.5) m
Maximum coverage radius, (r_m)	4 m
VLC transceiver parameters	
Average output optical power	10 W [1,20]
FoV of the PD	60° [1,20]
Gain of the optical filter	Unity Gain [1,20]
Gain of the transmission band-pass filter	Unity Gain [1,20]
LED and reflective element tilt and rotation angles ($\beta_i, \alpha_i, \beta_w, \alpha_w$)	U[90°,180°] [1]
LED semi-angle, ($\Phi_{i1/2}$)	60° [1,20]
Number of PDs	1
Number of scatterers, (N)	40 [1]
Obstacle intensity parameter, (ϵ)	5 per minute [1]
PD height	1.8 m
PD physical active area (A_p)	1 cm^2 [1,20]
Reflective element area, (ΔA_w)	1 cm^2 [1,20]
Reflective element position (x_w, y_w, z_w)	(3,3,2.5) m
Responsivity	0.53 A/W [1,20]
Wall reflection coefficient, (ρ_w)	0.6 [1,20]
Signal parameters	
Sampling rate	2 samples/bit [14]
Modulation scheme	OOK [14]
Transmission rate	100 Kbps [14]
Optical watch	200 kHz [14]
Frame length	24717 bits [14]
Number of frames	122 [14]
Estimation sequence length	24 bits [14]

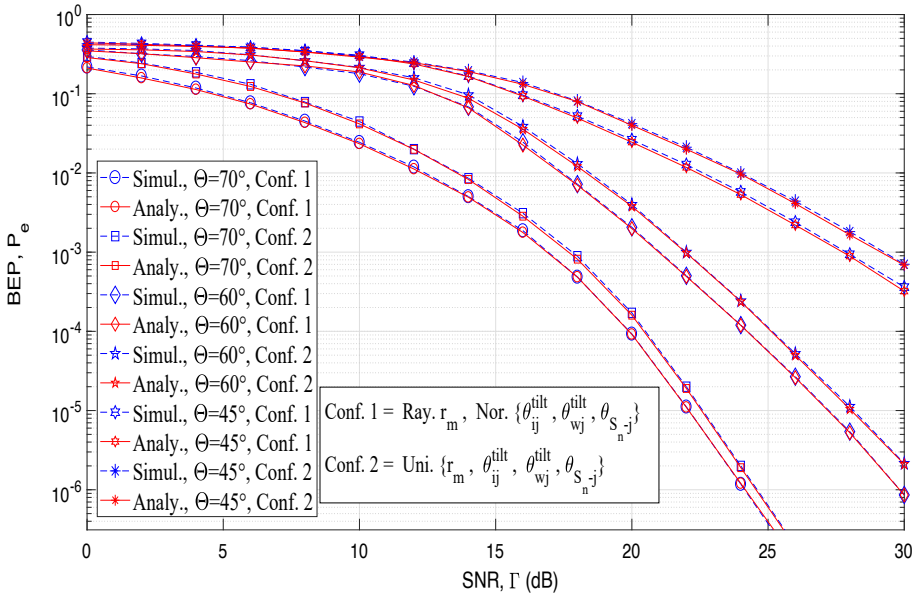

Fig. 2. BEP versus the average SNR per symbol with perfect CSI.

3. BEP analytical derivation

Based on the IEEE 802.15.7 standard and using PHY-I mode [14], we consider OOK modulated symbols such that $s \in \{0, A\}$, as well as perfect and imperfect CSI.

3.1. BEP expression for perfect CSI

The average BEP for the OOK modulation implemented in the UM-VLC system is given as $P_e = \int_0^\infty Q\left(\sqrt{\frac{\Gamma}{4}\varphi}\right) f_{h_m^2}(\varphi) d\varphi$ [16], where $\Gamma = \frac{A^2}{(\sigma_s^2+\sigma_t^2)}$, φ is the argument of the PDF. which represents the value h_m^2 takes, and $Q(\cdot)$ is the Q-function, which can be rewritten using the approximation $Q(\nu) \approx \frac{1}{12}\exp\left(\frac{-\nu^2}{2}\right) + \frac{1}{4}\exp\left(\frac{-2\nu^2}{3}\right)$ [19] as $Q\left(\sqrt{\frac{\Gamma}{4}\varphi}\right) = \frac{1}{12}\exp\left(-\frac{\Gamma}{8}\varphi\right) + \frac{1}{4}\exp\left(-\frac{\Gamma}{6}\varphi\right)$. By adopting the previous assumption in P_e, and integrating it in the interval $[h_{m(min)}, h_{m(max)}]$, where $h_{m(min)}$ and $h_{m(max)}$ depend on the ranges of the random variables values in h_m, the closed analytical expression for the BEP is given as

$$P_e = \left\{ \frac{\sqrt{\pi}}{8} \left[\frac{\mathrm{erf}\left(\sqrt{\alpha_1\varphi}\right)}{3\sqrt{\alpha_1}} + \frac{\mathrm{erf}\left(\sqrt{\alpha_2\varphi}\right)}{\sqrt{\alpha_2}} \right] f_{h_m^2}(\varphi) \right\} \Big|_{h_{m(min)}}^{h_{m(max)}}, \tag{16}$$

where $\alpha_1 = \Gamma/8, \alpha_2 = \Gamma/6$, and $\mathrm{erf}(\cdot)$ is the error function.

3.2. BEP expression for imperfect CSI

Based on the sub-optimal structure of the VLC system with imperfect CSI, described in Section 2.3, the BEP for OOK modulation by using LS is given as

$$P_{e,ls} = Pr\{r\hat{h}_{m_{ls}} < 0\} \tag{17}$$

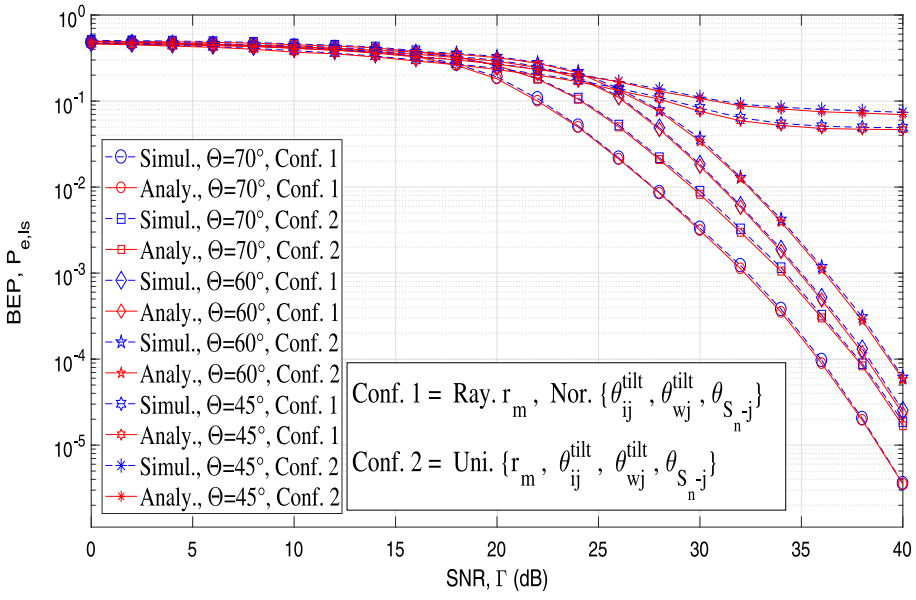

Fig. 3. BEP versus the average SNR per symbol with imperfect CSI and $\Gamma_s = 15$dB.

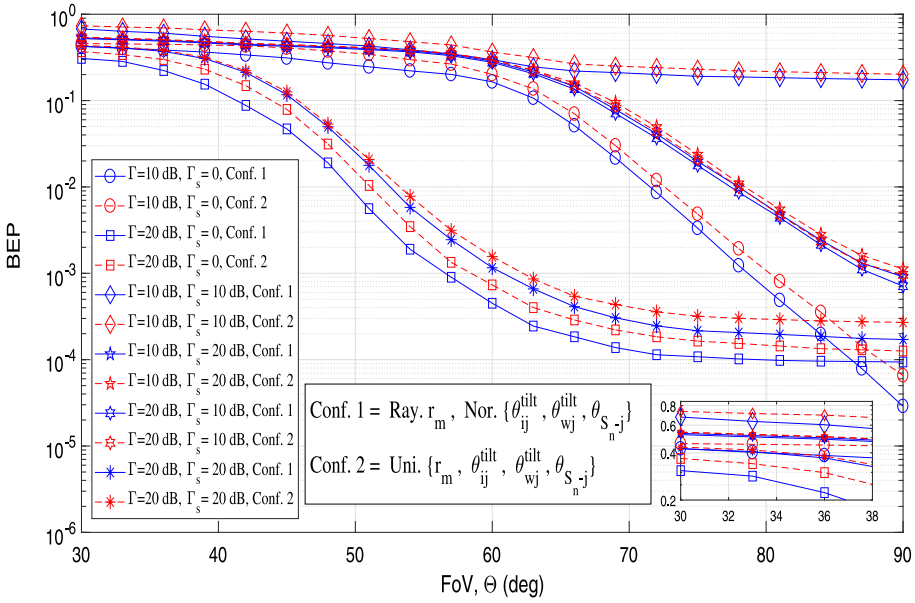

Fig. 4. BEP versus FoV of the LED with perfect and imperfect CSI.

$$= \int_0^{\infty} \left[Q\left(\sqrt{\frac{\Gamma}{4}\varphi}\right) + Q\left(\sqrt{\Gamma_s \varphi}\right) - 2Q\left(\sqrt{\frac{\Gamma}{4}\varphi}\right) Q\left(\sqrt{\Gamma_s \varphi}\right) \right] f_{h_m^2}(\varphi)\, d\varphi. \tag{18}$$

Assuming independence of the noise samples over time, n_m and ξ_{ls} are independent variables. Therefore, using the Q-function approximation [19], we obtain the closed expression of $P_{e,ls}$ as

$$\begin{aligned} P_{e,ls} &= P_e + \left\{ \frac{\sqrt{\pi}}{8} \left[\frac{\operatorname{erf}\left(\sqrt{\alpha_3 \varphi}\right)}{3\sqrt{\alpha_3}} + \frac{\operatorname{erf}\left(\sqrt{\alpha_4 \varphi}\right)}{\sqrt{\alpha_4}} \right. \right. \\ &\quad - \frac{\operatorname{erf}\left(\sqrt{\alpha_5 \varphi}\right)}{18\sqrt{\alpha_5}} - \frac{\operatorname{erf}\left(\sqrt{\alpha_6 \varphi}\right)}{6\sqrt{\alpha_6}} - \frac{\operatorname{erf}\left(\sqrt{\alpha_7 \varphi}\right)}{6\sqrt{\alpha_7}} \\ &\quad \left. \left. - \frac{\operatorname{erf}\left(\sqrt{\alpha_8 \varphi}\right)}{2\sqrt{\alpha_8}} \right] f_{h_m^2}(\varphi) \right\} \Bigg|_{h_{m(\min)}}^{h_{m(\max)}}, \end{aligned} \tag{19}$$

which is conditioned by the gain and the statistics of h_m^2, as well as by the statistics of n_m and ξ_{ls}. The respective constants' values are: $\alpha_3 = \Gamma_s/2$, $\alpha_4 = \Gamma_s/3, \alpha_5 = \Gamma/8 + \Gamma_s/2, \alpha_6 = \Gamma/8 + \Gamma_s/3, \alpha_7 = \Gamma/6 + \Gamma_s/2$, and $\alpha_8 = \Gamma/6 + \Gamma_s/3$.

4. Numerical Results and Discussion

In this Section, computer simulations are presented to validate the analytical expressions given in (16) and (19). To evaluate and analyze the effects of the variables that characterize the system, we simulated various UM-VLC scenarios using different random probability distributions; where θ_{ij}^{tilt}, θ_{wj}^{tilt}, and $\theta_{S_n-j}^{tilt}$ are characterized by $\mathcal{N}(30°, 20°)$ or $\mathcal{U}[20°, 40°]$, and r_m is given by $\mathcal{R}(2)$ m. or $\mathcal{U}[0,5]$ m., for both perfect and imperfect CSI [16]. The most important parameters used in the simulations and the UM scenario size are summarized in the Table 1.

Fig. 2 illustrates the BEP versus average SNR per symbol curves for the UM-VLC system with perfect CSI. The analytical BEP was obtained for different FoV values, by varying the probability distributions of r_m, θ_{ij}^{tilt}, θ_{wj}^{tilt}, and $\theta_{S_n-j}^{tilt}$. The analytical BEP curves obtained using (16) agree well with the simulated curves using Monte Carlo simulations. Furthermore, it is observed that the UM-VLC system performance degrades when the FoV decreases for any of the probability distributions of the involved variables.

Fig. 3 depicts curves of the BEP versus average SNR per symbol for the UM-VLC system with imperfect CSI employing LS estimation and considering $\Gamma_s = 15$dB [5]. As in Fig. 2, the BEP increases when the FoV values decrease for all probability distributions analyzed. The analytical BEP curves obtained using (19) agree well with the simulated curves using Monte Carlo simulations. In general, the BEP of the UM-VLC system with imperfect CSI are lower compared to the UM-VLC system with perfect CSI. Finally, it is interesting to note that some BEP curves saturate for higher values of Γ due to lower values of Θ, specifically in the case of $\Theta = 45°$.

Finally, Fig. 4 depicts the analytical curves of BEP versus Θ considering perfect and imperfect CSI employing LS estimation and several values of Γ and Γ_s. In general, it is noted that with higher Θ values, the system performs better. Furthermore, the performance increases significantly for higher values of Γ and Γ_s, whereas for lower Θ,Γ, and Γ_s values, the performance of the system is almost identical. We can also observe that the saturation of some BEP curves tends to be prominent due to higher values of Γ_s.

5. Conclusion

In this manuscript, statistical expressions for the UM-VLC square-channel gain components, as well as the analytical expressions for the BEP are obtained. A close agreement is observed between the analytical and simulated curves, which verifies the effectiveness of the analysis presented. The performance of the system mainly depends on the position and orientation of the receiver, as well as shadowing, which are analyzed using various PDF expressions. In general, the system performs better for higher values of FoV. We also note a slight dependence of the system considering perfect CSI and LS estimation for lower FoV values. Whereas for higher FoV values, the performance of the system depends on the precision of the channel estimation technique. In the case of the UM-VLC system with perfect CSI, a value of $\Theta = 70°$ generates the best performance in terms of BER for both random distributions of the variables of interest (Normal and Rayleigh). This effect is due to the direct dependence of the channel components with Θ. On the other hand, in the case of the UM-VLC system with imperfect CSI, the values of $\Theta = 70°$ and $\Theta = 45°$ generate the best and worst performance of the UM-VLC system, respectively. In this case, there is also a direct dependence in terms of the values of Γ and Γ_s used. The saturation of various BER curves is more prominent for a value of $\Gamma_s = 20$dB, due to its limiting effect on the performance of the UM-VLC system. As future work, the

analysis of the UM-VLC MIMO system and the experimental validation of the theoretical expressions and analytical results found in this article are considered. This validation will be developed after implementing an experimental UM-VLC test-bed that emulates the physical characteristics of underground mines. In this sense, the experimental UM-VLC test-bed will be implemented using VLC transceivers, electro-optical components, and a prototype to emulate real conditions within UM tunnels.

Declaration of Competing Interest

The authors declare that they have no known competing financial interests or personal relationships that could have appeared to influence the work reported in this paper.

Acknowledgments

This work was supported by ANID FONDECYT Regular No. 1211132, Doctoral Fellowship Grant from ANID PFCHA/Doctorado Nacional/2019–21190489, CODELCO: Concurso Piensa Minería 2021, UDLA Telecommunications Engineering Degree, SENESCYT "Convocatoria abierta 2014-primera fase, Acta CIBAE-023–2014", and Grupo de Investigación en Inteligencia Artificial y Tecnologías de la Información (IA&TI).

References

[1] Palacios P, et al. A VLC Channel Model for Underground Mining Environments With Scattering and Shadowing. IEEE Access 2020;8:185445–64. https://doi.org/10.1109/ACCESS.2020.3030615.
[2] Palacios P, et al. Interference mitigation for visible light communications in underground mines using angle diversity receivers. Sensors 2020;20(2):367.
[3] Gupta A, Garg P. Statistics of SNR for an Indoor VLC System and Its Applications in System Performance. IEEE Commun Lett 2018;22(9):1898–901. https://doi.org/10.1109/LCOMM.2018.2859990.
[4] Hosney M, et al. Interference Mitigation Using Angular Diversity Receiver With Efficient Channel Estimation in MIMO VLC. IEEE Access 2020;8:54060–73. https://doi.org/10.1109/ACCESS.2020.2981137.
[5] Mohapatra S, Satapathy G, Dash SP, Sahu PR. Performance Analysis of Visible Light Communication System With Imperfect CSI. IEEE Commun Lett 2020;24(12):2844–8. https://doi.org/10.1109/LCOMM.2020.3016044.
[6] Sekhar KR, Miramirkhani F, Mitra R, Turlapaty AC. Generic BER Analysis of VLC Channels Impaired by 3D User-Mobility and Imperfect CSI. IEEE Commun Lett 2021;25(7):2319–23. https://doi.org/10.1109/LCOMM.2021.3068051.
[7] Reddy Sekhar K, Mitra R. MBER Combining for MIMO VLC With User Mobility and Imperfect CSI. IEEE Commun Lett 2020;24(2):376–80. https://doi.org/10.1109/LCOMM.2019.2954496.
[8] Wang J, Al-Kinani A, Sun J, Zhang W, Wang CX. A path loss channel model for visible light communications in underground mines. In: IEEE/CIC International Conference on Communications in China (ICCC), IEEE; 2017. doi:10.1109/iccchina.2017.8330479.
[9] Wang J, Al-Kinani A, Zhang W, Wang C. A new vlc channel model for underground mining environments. In: 2017 13th International Wireless Communications and Mobile Computing Conference (IWCMC); 2017. p. 2134–9.
[10] Cespedes MM, Armada AG. Characterization of the visible light communications during the construction of tunnels. In: 2019 16th International symposium on wireless communication systems (ISWCS), IEEE; 2019. doi:10.1109/iswcs.2019.8877189.
[11] Zhai Y, Zhang S. Visible light communication channel models and simulation of coal workface energy coupling. Math Problems Eng 2015;2015:1–10. https://doi.org/10.1155/2015/271352.
[12] Wang J, Al-Kinani A, Zhang W, Wang C-X, Zhou L. A general channel model for visible light communications in underground mines. China Commun 2018;15(9):95–105. https://doi.org/10.1109/cc.2018.8456455.
[13] Riurean S, Stoicuta O, Leba M, Ionica A, Rocha Á. Underground channel model for visible light wireless communication based on neural networks. In: World Conference on Information Systems and Technologies. Springer; 2020. p. 293–305.
[14] IEEE Standard for Local and metropolitan area networks–Part 15.7: Short-Range Optical Wireless Communications, IEEE Std 802.15.7-2018 (2019) 1–670.
[15] Dixit V, Kumar A. An exact BER analysis of NOMA-VLC system with imperfect SIC and CSI. AEU-Int J Electron Commun 2021;138:153864.
[16] Eroglu YS, Yapici Güvenç Y. Impact of Random Receiver Orientation on Visible Light Communications Channel. IEEE Trans Commun 2019;67(2):1313–25. https://doi.org/10.1109/TCOMM.2018.2879093.
[17] Springer MD, Thompson W. The distribution of products of independent random variables. SIAM J Appl Math 1966;14(3):511–26.
[18] L-Garcia A, Probability, Statistics and Random Processes for Electrical Engineering; 2008.
[19] Elamassie M, Miramirkhani F, Uysal M. Performance Characterization of Underwater Visible Light Communication. IEEE Trans Commun 2019;67(1):543–52. https://doi.org/10.1109/TCOMM.2018.2867498.
[20] Ghassemlooy Z. Optical Wireless Communications: System and Channel Modelling with MATLAB. Boca Raton, FL: CRC Press; 2018.